Response to Reviewer #1

One place where I was confused was caused by not realizing the nature of how the solutions were derived, numerically using Equations 6, 7 and 8, apparently, as stated in the appendix. I didn't at first notice a reference to the appendix in the text.... after searching for it, I see it is referenced on page 7. It may be that the main body of the text needs a more forthright statement about what is done to produce the results, and a "louder" statement of what Appendix A is about would be helpful to some readers.

In a revised manuscript, I have made a significant effort to address this concern. I have added text at the beginning of Section 3 that clarifies the modeling approach. I've also incorporated the Appendix into the main text in a way that is more clear for the reader. I have also reorganized subsections (and sub-subsections) in Sections 3 and 4 so that the paper outline offers a better guide of the calculations that are presented. I have also added several "signposts" throughout the manuscript that attempt to orient the reader.

I think it is important to state somewhere at the outset and also in regard to future research that the fern-structure of the ice shelf may have additional bearing on the problem. In this case, the "touching of the top" is by weak, crushable firn. Also parts of the ice shelf that are in snow accumulation areas will have rift tops that are being actively filled with new material. Dealing with this is far beyond the scope of the present paper, but it worth identifying as a factor in future investigation.

Agreed. In a revised manuscript I have now explicitly mentioned the role of firn and its approximation in my model. I found the most natural place for this clarification to be at the beginning of the discussion section.

I am very impressed with the fact that observations, specifically (1) the absence of seismicity at rift tips, (2) the failure of a wave-forced propagation of a Nascent rift, and (3) the view of the compressive arch by Doake, are so nicely explained by the simple analysis of the theory presented. This, to me, is a great success and one which suggests that this approach may be what breaks any "log jam" over how rifting on ice shelves is to be pursued in the future.

Thank you!

Around line 30 of page 2. I wonder if a citation to a paper by Sanderson would be appropriate. He thought about ice-shelf margins. Journal of Glaciology, V22, 1979.

Sanderson was previously cited in my manuscript but not on this point. I have added this reference at this location as suggested.

Is equation 2 the bending moment due to the stress balance at the ice front that leads to a bending moment? Just a comment would suffice.

Yes, that's right. I've tried explaining this slightly differently in the text.

In the discussion along with Figure 1, it may be useful to point the reader to observational studies of rift walls: e.g., Scambos, T., Ross, R., Haran, T., Bauer, R., Ainley, D., Seo, K., . . . MacAyeal, D. (2013). A camera and multisensor automated station design for polar physical and biological systems monitoring: AMIGOS. Journal of Glaciology, 59(214), 303-314. doi:10.3189/2013JoG12J170 Note figure 8 in that paper.

I'm grateful to the reviewer for pointing out this reference. I've added a mention to it.

In describing the model, I think it is important to state whether a firn layer is going to be treated or not.

I do believe that treating the firn layer is beyond the scope of the present paper. Since the firn layer may nevertheless be of importance, I have added text stating this point at the beginning of Section 3.1 as well as in the Discussion section.

Also, although a minor point: I wonder if it is worth mentioning that brine-infiltration, horizontally along the bottom of the firn where it is permeable and where there is an ice front or rift wall might introduce secondary effects on rift wall bending moments etc..

I have made additional note of this process (start of Section 5).

page 9 just below line 185. f is given to 4 significant digits. I wonder if this could be considered misleading. I also note that the Young's modulus that is used in the study is expressed as if it were very accurately known. My understanding is that relative sizes are more likely to be significant in terms of what readers take away from the comparison t this point in the paper. Perhaps that should be stated.

I have changed this mistake. Significant digits are now consistently reported.

Figure 5, and some of the preceding figures. Do these results present the solution of Equations 6 7 and 8? I'm confused as to the specific process required to generate the curves and 2-d plot of displacement and other factors. A simple summary (before the results are presented) that describes how the model is implemented would be helpful to other researchers. Oh Dear! I see that this is all explained in the Appendix. (I should have noticed!) But, if my confusion (missing the reference to the appendix) can be of service in improving the exposition, let it so be.

Yes, this is useful. Again, as noted in the first comment above, I have made a significant effort to clarify the exposition.

Response to Reviewer #2

- What is the value the author uses for the critical stress intensity factor Kc? In the text, there is no explicit value given.

Following the work of Rist et al (2002), I use 100kPa m^{1/2}. None of the results in the manuscript are sensitive to this precise value. I have added text at the end of Section 3.2 that provides this information.

- Could the author please include the text of both appendices in the main text? The points that are discussed there are critical for the comprehension of the paper.

Yes, I have moved the text in the Appendix to the main text.

There is no reference to the Appendix and it is not directly clear, for instance, why the author uses the displacement in one direction only dependent on one critical stress factor of a certain loading mode (displacement direction method).

It is simply a matter of definition that each mode depends on an orthogonal component of displacement. This definition, however, bears utility in its relationship to fracture propagation. I have modified the text in Section 3.2 following the definitions of the stress intensity factors to explain this point.

The author can also shortly discuss that this method/approximation has first-order accuracy.

I have made such a note.

- At the moment it is also not clear which equations the author uses for the numerical finite element and which only for the analytical solution.

Following on the comments from Reviewer #1, I have made changes to the manuscript in an effort to improve clarity on exactly this point. I have added the exact equations that are solved in Section 3.1. I have also added text at the beginning of Section 3 that clarifies the modeling approach.

For instance, Eqs. (1)-(3) are only used for the analytical solution. Is this right?

Yes, and I have added a note to this extent in Section 3.1.

For the numerical solution, the displacement field can be derived with three-dimensional elasticity and the different boundary conditions and then in a post-processing step the stress

intensity factors are computed out of the displacement field. Then the author should mention this procedure in the text that it is directly clear for the reader. Maybe it is then also better to solve Eqs. (6)-(8) for the stress intensity factors: KII(z)=: : :.

Yes, that is exactly correct. I have added a note that clarifies this point in the introduction as well as at the beginning of Section 3.

- Does the author also consider rifts that are not filled by water? The water cannot percolate in all rifts occurring in an ice shelf, for example, if the rift is too far away from the ice front also dry (not filled by ocean or melt water) rifts can exist. How is the stability of dry rifts? Maybe the author can also add a short comment on these studies in the text.

This is an interesting point and I have made mention of it at the beginning of Section 5.

- Figure 3: the arrows for mode II should also be plotted at the rift edges as the author did it for mode I and mode III.

I've made this change.

- What is the minimum element size along the rift? Did the author a mesh convergence study to also verify that the results are not mesh dependent (a crucial check if one would consider stress intensity factors at the crack tip).

Yes, this is an important point. I did verify that the results are not mesh-dependent prior to initial submission. The maximum element size near any boundary, including the rift tip, is constrained to be no greater than h/16 with ice thickness h. Furthermore, stress intensity factors are measured over several elements, an essential aspect of mesh independence. Although some of these points were already described in the text, I have added more detail in the newly-created Section 3.2.2.

Specific comments and questions:

- Eq. 6-8: I do not have access to the Tada et al. 2000 paper, but are the factors in these equations right? I found in Gupta et al. 2017 ("Accuracy and Robustness of Stress Intensity Factor Extraction Methods for the Generalized/eXtended Finite Element Method") sqrt(r/(2*pi)) and mu/(4-4*nu). Could the author please check the equations.

I'm grateful for the reviewer's attention to detail for catching this mistake. I verified that these equations were correctly implemented in my finite element calculation. It appears that this mistake was entirely limited to the manuscript and the appropriate correction has been made.

- Equations: Why do the author sometimes use an equality sign and sometimes the sign for identical statements with three strokes above the other (see Eqs. (2) and (3))? For example, Eq. (1) and Eq. (4) are both statements how the stress component or the stress tensor for the boundary condition is computed.

I use the symbol with three lines to denote a definition. I've checked that this is consistently used in all equations and also made a note for the reader.

l.58: the traction boundary condition should be zero (stress-free boundary due to zero pressure) at the top of the ice shelf. The author only gets non-zero values as the simplified assumptions of Weertman and Reeh are used. Here, a comment that these results are not necessary for the finite element formulation could be helpful for the understanding of this paper.

Yes, agreed. I added a sentence clarifying this point in Section 3.2.1.

l.93 and Fig. 2: The geometry of the rift in the figure looks like a rhomb, but in the text the rift is described with a uniformly 10 m width and only near the rift tip it is tapered. Could the author update the figure that it fits to the description of the rift? The author already states in the caption that the width and shape are exaggerated but if the author could also include the width of only 10 m in the figures, it will be clearer that LEFM could be applied where an infinitesimal small crack tip is absolutely necessary.

I have updated Figure 2 as the reviewer suggests.

l. 98: Is the perturbation stress tensor the deviatoric stress tensor? Can the author also include the word deviatoric to make it directly clear for everyone and maybe add at the end of the sentence "times identity tensor"? Eq. (4): Why is the pressure boundary condition only applied for the deviatoric stress tensor and not as common to the total (Cauchy) stress tensor?

Briefly, no, it is not the deviatoric stress tensor. The perturbation tensor is T- p_0 whereas the deviatoric tensor is T-p. As this is an important point, I explain the difference in detail in the beginning of Section 3.1. The perturbation tensor still allows for elastic compressibility whereas the deviatoric stress tensor does not.

Figure 3: Could the author please add a legend to the plots A, B, D, E? Could the author please also use capital letters for the reference to the figures, see for instance l.154,155.

I have made these changes.

Why does the author choose slightly different density values of 0.9 (l.55) and 0.89 (l.263)?

This was an oversight. In the revisions I've opted to use the value with fewer significant figures to reflect the uncertainty in this quantity.

l. 265: What are the boundary conditions for the case studied in Fig. 3? At each boundary water pressure?

I have clarified the figure caption to state that this figure is drawn for a marginal rift in a floating ice tongue.

Why are all computed values of this geometrical factor negative in Table A1 (2D and 3D)? Is this due to the boundary conditions acting in an embayment?

Yes, this is for an embayment geometry. I have added this clarifying point to the text.

Does this statement mean that a rift longer than 217m will never be stable in a free-floating ice shelf?

This comment prompted a change to how stability is evaluated in my manuscript. In the revised manuscript, I have introduced the optimally oriented stress intensity factor. I have also removed this calculation as I do not believe it is consistent the three-dimensional results.

Fig. 1: The author should add in the caption of this fuigure that the boundary conditions on the side of the ice shelf are too far away to have an influence on the rift. If this is not the case, then the bending moment of the water pressure at the side counteract the closure of the rift top by the opening of the rift.

I have made such a note.

Fig. 4: Why are the orange and blue curves for alpha»0.5 not reaching or converging to the red curve? The boundary conditions of free slip or water pressure are in this case far away from the rift and therefore the difference of all three cases should be minimal.

This is a real effect. An essential aspect of LEFM is that distant boundaries may still alter energy release rates. This statement is epitomized by the J-Integral of Rice (1968), which expresses the energy release rate as an integral over all boundaries.

Fig. 6B: Shows the red curve in this figure not an unstable rift if alpha is in between 0.1 and 0.3? For the stress intensity factor of the shearing mode (Mode-II) it is sufficient for rift propagation that the magnitude is greater than 1 (cf. l. 228).

I have revised the previously-numbered Fig 6. It and previously-numbered Fig 4 both now show the optimally-oriented SIF. As described in the text Section 3.8, the optimally-oriented SIF provides a better measure of stability. More directly to the reviewer point, I have also modified

the discussion in (newly-numbered) Section 4.2 and 5.1 to give a more subtle description of the regimes of propagation.

Technical corrections. I have addressed each of the small technical corrections brought up by the reviewer.

Ice shelf rift propagation: stability, ~~three dimensional~~ three-dimensional effects, and the role of marginal weakening

Bradley Paul Lipovsky

Department of Earth and Planetary Sciences
Harvard University

Correspondence: brad_lipovsky@fas.harvard.edu

Abstract. Understanding the processes that govern ice shelf extent are of fundamental importance to improved estimates of future ~~sea level~~ sea-level rise. In present-day Antarctica, ice shelf extent is most commonly determined by the propagation of through-cutting fractures called ice shelf rifts. Here, I present the first three-dimensional analysis of ice shelf rift propagation. I present a linear elastic fracture mechanical (LEFM) description of rift propagation. The model predicts that rifts may be stabilized when buoyant flexure results in contact at the tops of the near-tip rift walls. This stabilizing tendency may be overcome, however, by processes that act in the ice shelf margins. In particular, both marginal weakening and the advection of rifts into an ice tongue are shown to be processes that may trigger rift propagation. Marginal shear stress is shown to be the determining factor that governs these types of rift instability. I furthermore show that rift stability is closely related to the transition from uniaxial to biaxial extension known as the compressive arch. Although the partial contact of rift walls is fundamentally a three-dimensional process, I demonstrate that it may be parameterized within more numerically efficient two-dimensional calculations. This study provides a step towards a description of calving physics that is based in fracture mechanics.

1 Introduction

The Antarctic ice sheet is projected to loose mass this century. Although the rates of mass loss over this timeframe are typically projected to mirror recent rates, several types of more extreme ice sheet response to global climate forcing cannot presently be excluded (**?**). Perhaps the most prominent of these extreme changes is the retreat of the floating ice shelves that fringe the Antarctic continent. Ice shelf retreat has been observed to occur gradually, i.e., over a period of years to decades (**??**), and also abruptly, i.e., over a period of weeks to months (**??**). Although ice shelves themselves do not contribute to ~~sea level~~ sea-level rise, they do act to buttress grounded ice (**????**). For this reason, ice sheet mass and therefore global mean ~~sea level~~ sea-level are closely connected to the extent and stability of ice shelves. Here, I examine the stability of ice shelves with respect to the propagation of large through-cutting fractures called rifts.

The largest modern ice shelves exist in embayments. This basic observation has long prompted the notion that embayments promote the existence of large stable ice shelves (**????**). Yet not all ice shelves fully fill the largest possible embayment. The Pine Island Glacier Ice Shelf, for example, does not presently fill the entire embayment between Bear Peninsula and Thurston Island; instead it fills the much smaller local embayment of Pine Island Bay. Furthermore, analysis of sediment cores ~~(?)~~ (**??**) and iceberg scour marks (**?**) suggest that past ice shelves have waxed and waned in extent through ice age cycles. Although embayments appear to stabilize ice shelves, it would therefore appear that some other process is responsible for determining the size of a stable ice shelf within a given coastal geometry. The close relationship between the state of stress in an ice shelf and the ice shelf boundary conditions ~~(??)~~ (**???**) motivates investigation into processes acting in ice shelf margins.

Ice shelf margins are the ~~region~~ part of the ice shelf grounding zone that is roughly parallel to flow (see Fig. **??**). The importance of ice shelf margins is suggested by several observations, foremost among these being the observation of marginal weakening prior to ice shelf collapse. Estimates of ice rheology based on the inversion of surface velocity fields show extensive marginal weakening prior to the collapse of the Larsen A (**?**) and Larsen B Ice Shelves (**??**). Although ice shelf collapse (i.e., total and rapid retreat) is a complex phenomenon that involves other processes besides rift propagation (**?**), rift propagation does appear to play a role in collapse. **?** explicitly noted that marginal weakening immediately preceded rift propagation and eventual collapse on Larsen B. Further observation of a relationship between ice shelf retreat, rifting, and marginal thinning has been noted in the Amundsen Sea Embayment (**?**) and Jakobshavn Isbrae, Greenland (**?**). Motivated by these observations, a central question of this paper is, what is the precise mechanical relationship between ice shelf margins and ice shelf rift propagation?

The main result of this paper is that marginal weakening can destabilize rift propagation. I begin by providing background on the state of stress in an ice shelf ~~as well as some aspects of linear elastic fracture mechanics (LEFM)~~ in Sections **??**~~and **??**~~. In Section **??** I describe three-dimensional elasticity calculations that are carried out using the finite element method and then post-processed to reveal fracture mechanical properties. A more precise statement of the main result is then given in Section **??**, where I also examine a simplified analytical treatment of the three-dimensional calculations. I conclude by discussing the relationship between rift propagation, the compressive arch, rift-filling melange, and ocean swell in Section **??**.

2 Background

I consider an ice shelf to be a buoyantly floating elastic plate of uniform thickness. ~~As such, a~~ Stress balance at the seaward-facing ice front ~~experiences~~ results in both a net bending moment and an in-plane horizontal membrane stress (**??**). The vertically-averaged membrane stress is,

$$\sigma_m \equiv \frac{\rho g h}{2}\left(1-\frac{\rho}{\rho_w}\right). \tag{1}$$

~~while the~~ I use the $\equiv$ symbol to denote a definition. The bending moment is given by,

$$m_0 \equiv \frac{\rho g h^3}{12}\left[3\left(\frac{\rho}{\rho_w}\right)-2\left(\frac{\rho}{\rho_w}\right)^2-1\right] \equiv \phi\frac{\rho g h^3}{12}. \tag{2}$$

In these expressions, ρ and ρ_w are the densities of ice and water and h is the ice thickness. Typical values of $\rho/\rho_w = 0.90$ give $\phi = 0.08$. The bending moment may also be expressed as a bending stress,

$$\sigma_b \equiv \frac{6 m_0}{h^2} = \phi\frac{\rho g h}{2}. \tag{3}$$

The bending stress σ_b is the value of the rift-normal stress at the top of the ice shelf; it is also the maximum value of the rift-normal stress. The horizontal component of loading (Eq. **??**) is commonly used as a boundary condition in numerical ice flow models, whereas the bending moment is not typically applied in ice sheet models because its effects are confined to a narrow boundary layer in the vicinity of the ice front (**?**).

Rifts walls have the same ice-front boundary conditions as a seaward-facing ice front. The main difference between a seaward-facing ice front and a rift wall is that it is possible for rift walls to come into contact. This contact is expected to occur at the top of the ice shelf and in the region near the rift tip, as illustrated in Fig. **??**b. Indeed, **?** recently observed that a rift tip on the Brunt Ice Shelf was further advanced at depth than at the surface, suggesting the occurrence of partial contact. I examine the partial contact of rift walls in Section **??**. As an aspect of linear elastic fracture mechanics, fracture wall contact is a well-studied topic ~~(**?**, Chapter 1, Part C)~~(**?**, Chapter 1, Section C).

I use ~~full~~ three-dimensional elasticity calculations combined with linear elastic fracture mechanics (LEFM) to examine the propagation of ice shelf rifts. Although a number of previous studies have examined ice shelf rifts using LEFM, no previous study appears to have considered three-dimensional effects. **?** calculated two-dimensional mixed mode (in-plane opening and shearing) stress intensity factors and as a result was able to state a fracture condition as well as predict rift propagation paths. Other ice shelf LEFM studies have mostly focused on propagation paths (**???**) and near-tip deformation (**??**).

A final point of background concerns the relationship between the forces that drive fracture and the background ice flow. In ~~real-world~~ real ice shelves, the state of stress is constantly evolving due to the change in geometry brought about by ice flow. Previous studies have examined the ~~flow–fracture relationship~~ relationship between ice flow and fracture in several ways. **?** carried out viscous flow calculations to constrain the state of stress in their elastic calculations. They then tuned elastic moduli and boundary conditions in their elastic calculations to match the observed viscous stresses. **?** parameterized a state of stress from a viscous flow model, but rather than tuning elastic moduli instead chose to introduce fictitious equivalent body

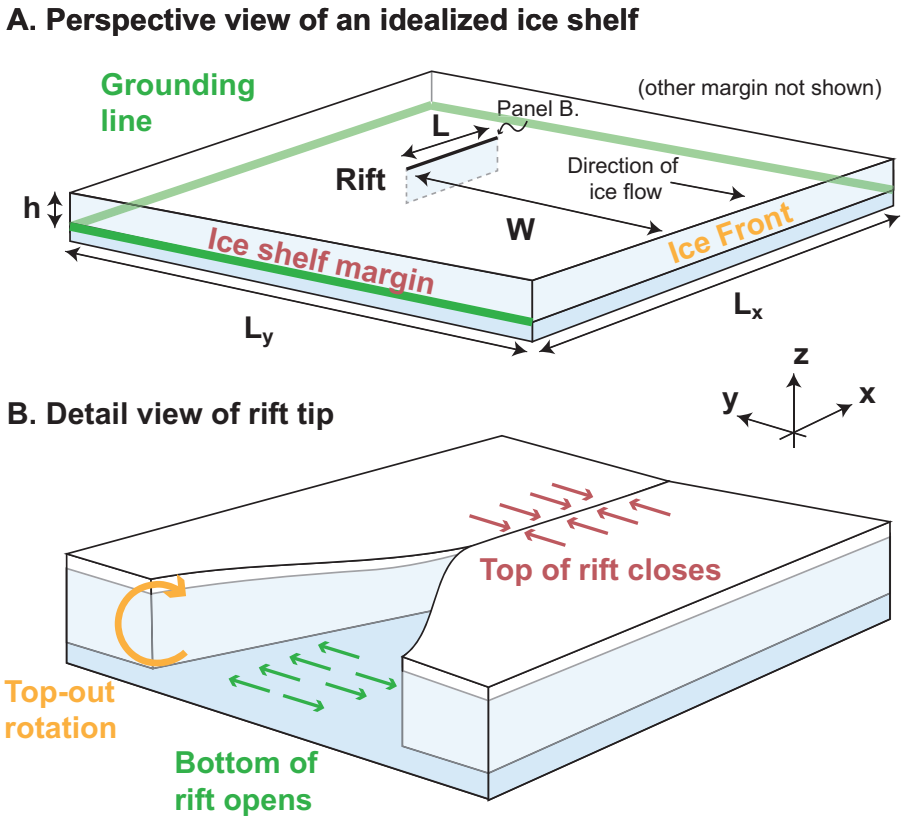

Figure 1. A. Simplified geometry of an idealized rectangular ice shelf. B. Zoomed in view of an ice shelf rift tip showing how buoyancy-driven rotation of the rift walls results in partial contact of the rift walls near the rift tip. Note that B. is drawn under the assumption that the rift tip is at least several flexural gravity wavelengths away from the ice shelf margin so that no flexural interaction occurs between these two regions.

forces. Here, I consider the hypothesis that the forces that drive rift propagation are entirely described by the instantaneous ice shelf geometry and boundary conditions. This hypothesis requires three-dimensional calculations in order to directly calculate –rather than parameterize or ~~approximate)~~ approximate– the role of gravitational driving forces. I ~~next~~ therefore continue to describe the details of ~~my mechanical~~ a three-dimensional elastic fracture model.

3 Mechanical Model

I begin this section by describing a three-dimensional elastic model of an ice shelf in which stresses and displacements are calculated using the finite element method (Sections **??** and **??**). I then describe a linear elastic fracture model which is closely related to these elasticity calculations (Section **??**).

3.1 Geometry

I consider the idealized ice shelf geometry shown in Fig. **??**. The ice shelf is square in map view (the x-y plane). The z axis is defined so that the positive z axis points upwards and the bottom of the ice shelf is located at $z = 0$. The ice shelf has horizontal dimensions $L_x = L_y = 100$ km and thickness $h = 200$ m. The ice shelf surface at $y = 0$ faces the ocean and the surface at $y = L_y$ faces the ice sheet. The surfaces at $x = 0$ and $x = L_x$ are referred to as the ice shelf margins. A single rift is located along the x axis at $y = W$. I treat two different general rift locations: marginal and central. These two rift locations are shown in Fig. **??**. I hold the rift length fixed at $L = 2.5$ km long for the marginal rift and $L = 5$ km long for the central rift.

Geometrically, I model a rift as a tapered rectangular hole in the ice shelf. Fractures in three dimensions have a fracture tip defined by a ~~two-dimensional~~ two-dimensional curve rather than a point. Although I refer to a rift tip for brevity, this term actually refers to a rift tip curve. In the treatment presented here, the rift tip curve is taken to be a vertical straight line. The rift is uniformly 10 m wide over most of its length. Simulations show negligible sensitivity to the choice of this width. Tapering is applied over a length equal to several widths (i.e., several tens of meters) near the rift tip.

3.2 Linear elasticity

I ~~solve~~ consider the equations of linear, homogeneous, isotropic, static, ~~three-dimensional elasticity (?).~~ three-dimensional elasticity (**?**),

$$\nabla \cdot \mathbf{T}' = -\rho \mathbf{g} \tag{4}$$

with total (Cauchy) stress tensor $\mathbf{T}'$, ice density ρ, and gravitational acceleration $\mathbf{g}$. Because I neglect any spatial variation in material parameters, my model does not include a firn layer.

I account for an initial hydrostatic stress in a manner following **?** wherein the equations of elasticity are solved for a perturbation stress tensor $\mathbf{T}$ defined as the total (Cauchy) stress tensor minus ~~hydrostatic pressure. The resulting boundary conditions (described below) are consistent with previous treatments of crevasse propagation in glaciers (e.g., ?). Terms reflecting the advection of prestress (?, Ch. 2, Eq. II-22) are found to be unimportant and are notdiscussed further. My use of isotropic elasticity implies the need for two elastic constants which I take to be Young's modulus $E = 9.7$~~the initial hydrostatic pressure,

$$\mathbf{T} \equiv \mathbf{T}' - p_0, \tag{5}$$

with,

$$p_0 \equiv \rho g (H - z) \tag{6}$$

The perturbation stress tensor is necessary for the following physical reason. Without subtracting the initial overburden pressure, the ice shelf experiences an initial volumetric contraction $\sim p_0/K$ with bulk modulus K. This volumetric contraction does not occur in real ice shelves because at time scales longer than the Maxwell time, ice is well approximated as being

incompressible (**?**). Note that the perturbation stress tensor is not equal to the deviatoric stress tensor defined as $\mathbf{T}' - p$. This difference is important because the perturbation stress tensor accurately captures permissible, elastic volumetric contraction, whereas the deviatoric stress tensor does not.

All three-dimensional elasticity calculations in this study are carried out with respect to this perturbation stress tensor. The equations of motion are,

$$\nabla \cdot \mathbf{T} = 0 \tag{7}$$

$$T_{ij} = K\delta ij\epsilon_{kk} + 2\mu(\epsilon_{ij} + \delta_{ij}\epsilon_{kk}/3), \tag{8}$$

$$\epsilon_{ij} = \frac{1}{2}\left(\frac{\partial u_i}{\partial x_j} + \frac{\partial u_j}{\partial x_i}\right). \tag{9}$$

The first of these equations describes momentum balance which is derived by combining Eq. (**??**) and (**??**). Eq. (**??**) describes the elastic constitutive relation (Hooke's Law) with shear modulus $\mu = 3.6$ GPa and Poisson's ratio $\nu = 0.3$~~, although I sometimes make use of the shear modulus $\mu \equiv E/(2+2\nu)$.~~. Although isotropic elasticity only requires two elastic moduli, for convenience I use Young's modulus $E \equiv 2\mu(1+\nu)$ and the bulk modulus $K = E/[3(1-2\nu)]$. Eq. (**??**) defines the strain tensor ϵ_{ij}. These equation use index notation with repeated indices implying summation, δ_{ij} denoting the Kronecker delta function, and the indices i, j taking values x, y, z.

3.3 ~~Boundary conditions~~

3.2.1 Boundary conditions

The ice front, rift walls, and top and bottom ice shelf surfaces are loaded by a depth-varying normal stress that is equal to the water pressure below the waterline and equal to zero above the waterline. These boundaries have zero applied shear stress. ~~I write this as a single condition on the stress tensor $\mathbf{T}$,~~ The water pressure condition may be written as,

$$\mathbf{n}^T \cdot (\mathbf{T}' \cdot \mathbf{n}) = -p - p_w(z), \tag{10}$$

with unit outward pointing normal vector $\mathbf{n}$, ice shelf draft $H_w \equiv \rho/\rho_w h$, and water pressure $p_w(z)$,

$$p_w(z) \equiv \begin{cases} \rho_w g\,[H_w - (z+w)] & z < H_w, \\ 0 & z \geq H_w. \end{cases} \tag{11}$$

Here, w is the vertical component of the displacement vector. This boundary condition is consistent with previous treatments of crevasse propagation in glaciers (e.g., **?**).

In all simulations that are presented here, the surface of the ice shelf above the grounding line at $y = L_y$ has a zero displacement boundary condition. Similarly, the ice shelf surface at the ice front at $y = 0$ has a water pressure boundary condition (Eq. **??**). In the margins, I examine three types of marginal boundary condition. These conditions are shown in Fig. **??**; they are:

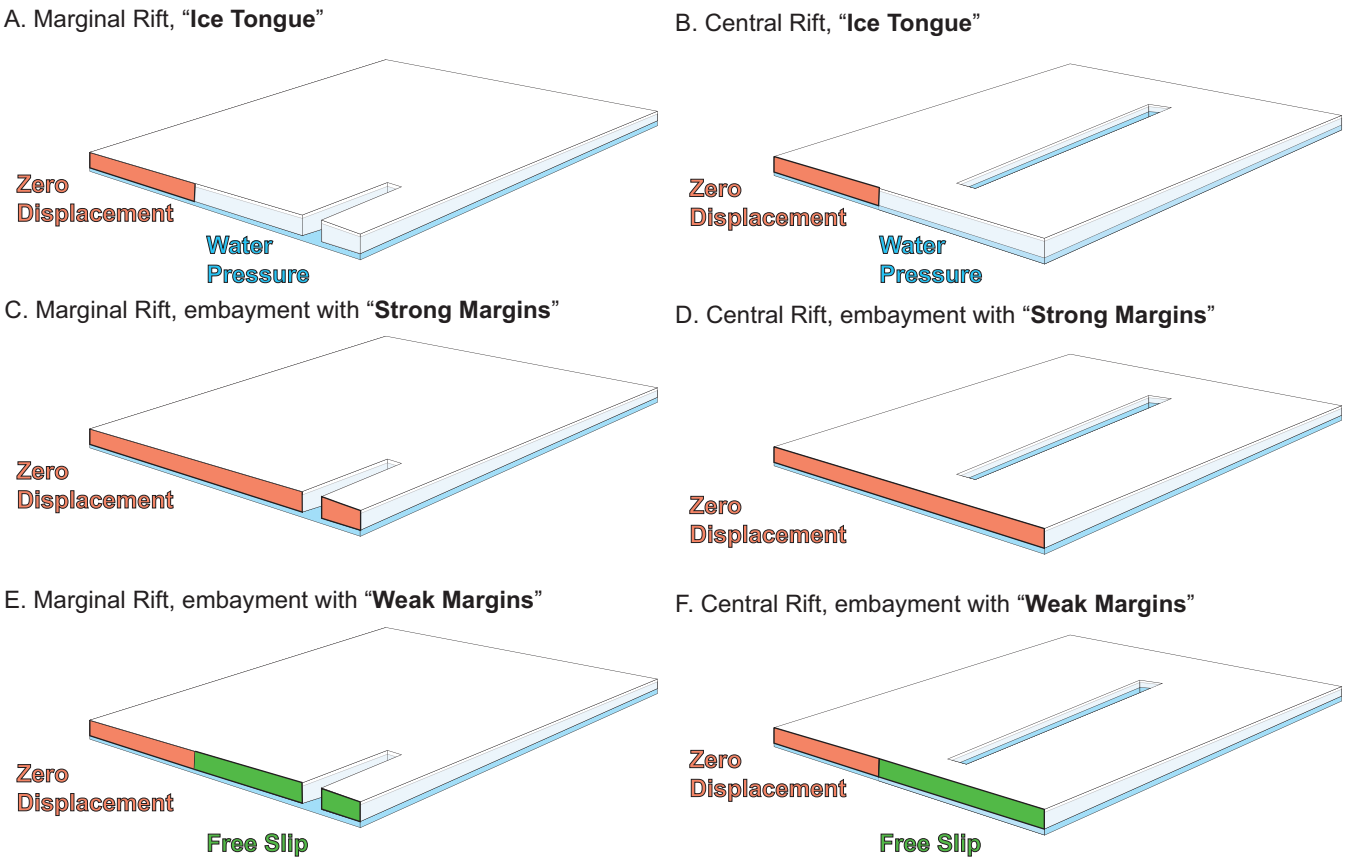

Figure 2. The geometries and boundary conditions considered in this study include: A. and B., ~~Margins half~~ Half zero displacement and half water pressure conditions; C. and D., ~~Entirely~~ entirely zero displacement conditions; and, E. and F., half zero displacement and half free slip conditions. I furthermore consider rifts that occur in the margins (A., C., and E.) and central rifts (B., D., and F.). The figures are not drawn to scale and the rift width ~~and shape are~~ is greatly exaggerated.

1. Ice shelf with ice tongue: margins have zero displacement between $y = L_y/2$ and $y = L_y$ and have water pressure between $y = 0$ and $y = L_y/2$;

2. Ice shelf in an embayment with strong margins: margins have zero displacement boundary condition; and,

3. Ice shelf in an embayment with weak margins: margins have zero displacement between $y = L_y/2$ and $y = L_y$ and have zero shear stress and zero normal displacement between $y = 0$ and $y = L_y/2$.

Note that Equations **??**-**??** occur naturally as a result of the more general three-dimensional boundary conditions. Equations **??**-**??** are not applied as constraints in the three-dimensional calculations. They are used, however, in Section **??** to analytically approximate the numerical results.

3.2.2 Numerical implementation

I solve Eqs. **??**-**??** using the finite element method. The ice shelf domain is discretized using a free tetrahedral mesh in three spatial dimensions or a free triangular mesh in two spatial dimensions. In the three-dimensional simulations, the maximum element size along the rift is set to be $m \equiv h/16$. The element size then increases away from the rift to a maximum value of 3.5 km. The rift is geometrically formed as a rectangular prism with width $W_{\text{rift}} = 10$ m and length L. I have verified that the results presented here have virtually no dependence on the choice of W_{rift} and m. In the two-dimensional simulations (described below), the maximum element size along the rift is $W_{\text{rift}}/10$.

3.3 Linear elastic fracture

~~Cracks –including rifts–~~ Fractures in elastic materials create displacement fields that vary proportional to the distance r from the crack tip as $r^{1/2}$ (**?**). The scalar constant of proportionality involves the stress intensity factor. Specifically, in terms of the displacement components u, v, and w corresponding to displacements in the x, y, and z directions, the stress intensity factors are defined through the relations (**?**),

$$u(r,z) = \frac{K_{II}(z)}{\mu/(2-2\nu)}\sqrt{2\pi r}\,4\frac{K_{II}(z)}{\mu/(1-\nu)}\sqrt{\frac{r}{2\pi}}, \tag{12}$$

$$v(r,z) = \frac{K_{I}(z)}{\mu/(2-2\nu)}\sqrt{2\pi r}\,4\frac{K_{I}(z)}{\mu/(1-\nu)}\sqrt{\frac{r}{2\pi}}, \tag{13}$$

$$w(r,z) = \frac{K_{III}(z)}{\mu}\sqrt{2\pi r}\sqrt{\frac{r}{2\pi}}. \tag{14}$$

~~In these expressions, r is the distance from the rift tip along the x-axis, μ is the elastic shear modulus and ν is the elastic Poisson ratio.~~

The quantities K_I, K_{II}, and K_{III} are the Mode-I, Mode-II, and Mode-III stress intensity factors (SIFs). The sense of motion associated with each mode of fracture is shown in Fig. **??**. ~~Although there is also an angular dependence to the near-tip displacement fields, I have suppressed this angular dependance by writing the displacements that occur on the fracture itself.~~ Equations **??**-**??** represent the asymptotic value, accurate to first order, of the displacement field near the rift tip on the plane of the fracture. The stress intensity factors bear a direct relationship to fracture propagation.

A basic tenet of fracture mechanics is that unstable crack growth occurs when the elastic strain energy available to drive fracture exceeds the energy required to create new fracture area (**?**). The key insight of linear elastic fracture mechanics is that this energy condition can be related to the stress intensity factors (**?**). ~~In three spatial dimensions, the energy release rate is (?),~~ The stress intensity factors may therefore be used as part of a fracture criterion. In this study, I examine mixed-mode fracture and I therefore use the theory of **?** that calculates the single optimally-oriented stress intensity factor from the three different stress intensity modes. This optimally-oriented stress intensity factor is the Mode I stress intensity factor along a plane oriented to minimizes K_{II} and K_{III} (**??**). Under the assumption (verified later) that K_{III} does not substantially contribute to the direction of propagation of the rift tip line, the Mode I stress intensity factor along the optimal angle of propagation θ can

be written as,

$$K_I^{Op} \equiv \cos\left(\frac{\theta}{2}\right)\left[K_I \cos^2\left(\frac{\theta}{2}\right) - \frac{3}{2}K_{II}\sin\theta\right]. \tag{15}$$

In this expression, the angle of propagation θ is given by,

$$G = \frac{K_I^2}{E/(1-\nu^2)} + \frac{K_{II}^2}{E/(1-\nu^2)} + \frac{K_{III}^2}{E/(1+\nu)} \quad \theta \equiv -2\tan^{-1}\left[\frac{-2K_I + 2\sqrt{K_I^2 + 8K_{II}^2}}{8K_I I}\right]. \tag{16}$$

~~Assuming that the Mode-I fracture toughness limits fracture behavior, we define the critical energy release rate~~

$$G_c \equiv \frac{K_{Ic}^2}{E/(1-\nu^2)},$$

~~with fracture criterion,~~

$$G > G_c.$$

In the adopted sign convention, negative angles indicate the direction pointing away from the ice front and straight-ahead propagation occurs when $\theta = 0$. Note that care must be taken in selecting the correct quadrant for the $\tan^{-1}$ function.

3.4 ~~Partial contact of rift walls~~

The fracture propagation criteria may then be stated as,

$$K_I^{Op} > K_{Ic}, \tag{17}$$

where the value $K_{Ic} = 100$ kPa$\sqrt{\text{m}}$, is the Mode I fracture toughness of ice (**?**). I refer to rifts that satisfy Eq. (**??**) as being unstable because they are expected to undergo some amount of propagation. Note that this does not necessarily mean that the rift will propagate in a way that will lead to a calving event. Propagation may stop, for example, before calving occurs. Rifts that do not satisfy Eq. (**??**) will be referred to as stable; such rifts are expected to close. This closure may result in partial contact of the rift walls, as discussed next.

3.3.1 Partial contact of rift walls

The partial contact of rift walls is a nonlinear phenomenon because it involves solving for the shape of the contacting region and therefore changing the region over which different boundary conditions are applied (**?**). Here, I treat a linear formulation of this problem wherein the Mode-I stress intensity factor K_I can take on positive or negative values. This situation is discussed in detail by **?**. For fractures with zero initial width, a negative K_I implies unphysical material overlap. I avoid this situation in my numerical simulations by giving the rift an initial ~~, nonzero opening (Appendix A)~~nonzero opening as described in Section **??**. This is consistent with the idea that rifts in ice shelves are probably not held open entirely by elastic stresses because they

have deformed through creeping flow. Other studies have shown that accounting for contact nonlinearity results in minimal differences from the linear problem for long fractures with $L \gg \lambda$ (**?**), where λ is the ice shelf flexural wavelength. Given that many rifts do reach lengths $L \gg \lambda$ (**??**), the linear approximation may well prove adequate for many cases of glaciological interest.

3.3.2 Stress intensity factor calculations

Stress intensity factors are calculated using rift wall displacements and Equations **??**-**??**. This evaluation method, essentially a post-processing step, is sometimes called the displacement correlation method (**?**) and has previously been used in glacier studies by **?**. I evaluate Equations **??**-**??** at a distance r from the crack tip that is at least several times m in order to achieve grid-size independence. In three dimensions, stress intensity factors are calculated at various heights through the ice shelf thickness, with the resulting calculations plotted in Fig. **??**.

4 Results and Analysis

~~Figure~~Fig. **??** shows a typical result of the finite element calculations. This figure shows that the Mode-I and Mode-III stress intensity factors are nearly linear with depth (i.e., Fig. **??**~~a, b~~A, B, and ~~e~~E), while the Mode-II stress intensity factor is nearly uniform with depth (i.e., Fig. **??**~~d~~D). This structure in the solutions permits an approximate parameterization of three-dimensional effects. Such a parameterization allows for a much less computationally costly, two-dimensional problem to be solved. ~~This parameterization is developed next , in Sections **??**.~~

I next develop the analytical parameterization (Section **??**). After developing this 2D parameterization, I then apply it to examine the relationship between rift position and rift stability. Some readers may wish to skip directly to ~~the discussion of marginal versus central rifts in Sections **??**and **??**~~these results, which are given in Section **??**.

4.1 Parameterization of 3D effects within 2D calculations

~~I now examine a simplified representation of the three dimensional finite element calculations that results in a parameterization for~~ The structure of the three-dimensional ~~bending effects. The analysis hinges on the linearity of the~~ stress intensity factors ~~and the associated principle of superposition. I first show that the Mode-I stress intensity factor is a superposition of bending and membrane loads, whereas the Mode-II and Mode-III stress intensity factors are entirely due to membrane loading and bending loads, respectively. The stress intensity factors may therefore be approximated as,~~ suggests the approximation,

$$K_I(z) = K_I^m + K_I^b \left(\frac{z - h/2}{h/2} \right), \tag{18}$$

$$K_{II}(z) = K_{II}^m, \tag{19}$$

$$K_{III}(z) = K_{III}^b \left(\frac{z - h/2}{h/2} \right), \tag{20}$$

where the superscripts b and m stand for bending and membrane, respectively.

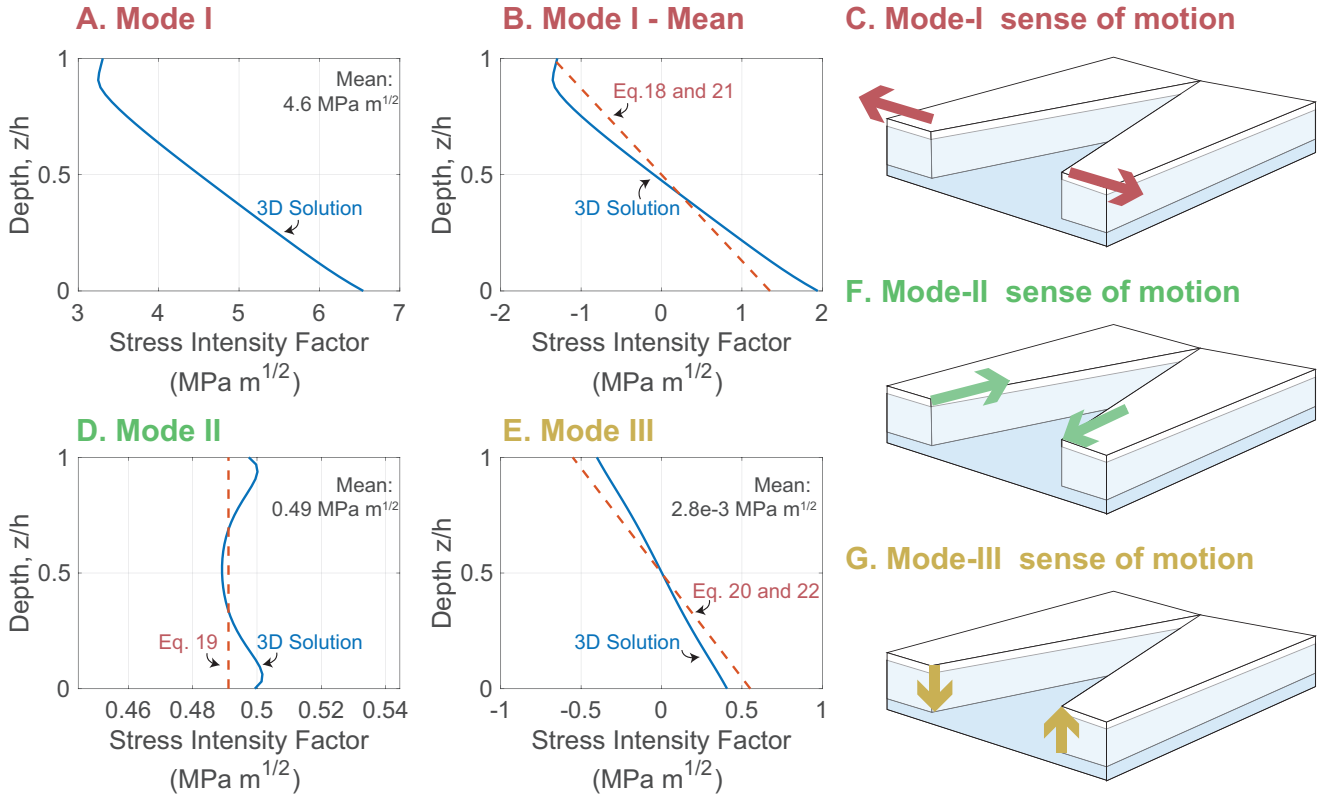

Figure 3. Typical three-dimensional stress intensity factors as a function of depth z in the ice shelf. A. and B. show the Mode I stress intensity factor K_I, D. shows the Mode II stress intensity factor K_{II} and E. shows the Mode III stress intensity factor K_{III}. The associated sense of motion for each mode is shown in panels C, F, and G. B. has the mean removed and is compared to the analytical solution of Eq. (??). The particular stress intensity factor solutions in these figures are plotted for a marginal rift in an ice tongue (i.e., the geometry shown in Fig. ??A.

~~I take the followingapproach to approximating the total, depth-dependent~~ In the following, I calculate the bending components of the stress intensity factors ~~. The bending terms~~ K_I^b and K_{III}^b ~~are calculated from analytical solutions, discussed below. The membrane terms~~ analytically and the membrane components K_I^m and K_{II}^m ~~, in contrast, are represented in terms of geometrical functions that directly reflect the finite element solution. These two approaches are discussed in greater detail in the following two subsections. The final result of Equations ?? - ?? are compared to full three-dimensional finite element solutions in Fig. ??.~~ using two-dimensional finite element solutions.

Table 1. Comparison between 2D and 3D calculations

	h	2D	3D	m	(2D-3D)/3D
χ	100 m	-0.2937	-0.3127	12.5 m	-6.1%
	200 m	-0.2937	-0.3012	5 m	-2.5%
	200 m	-0.2937	-0.3069	12.5 m	-4.3%
ψ	100 m	-0.04408	-0.0385	12.5 m	+14.5%
	200 m	-0.04408	-0.0382	5 m	+15.4%
	200 m	-0.04408	-0.0379	12.5 m	+16.3%

4.1.1 The bending components of ~~fracture~~the SIFs

I find that the bending component of the Mode-I stress intensity factor is well fit by the ~~simplified model~~ previously-published stress intensity factor solution (????),

$$K_I^b = -\sigma_b f(\nu)\sqrt{\lambda}. \tag{21}$$

Here, $\lambda^4 \equiv D/(\rho g)$ is the flexural length with flexural rigidity $D \equiv Eh^3/[12(1-\nu^2)]$~~, Youngs modulus E, and Poisson ratio ν~~. Hence, flexure results in a stabilizing contribution to the Mode I stress intensity factor that grows with ice thickness according to $K_I^b \sim h^{11/8}$. The bending stress σ_b is given by Eq. (??). The function $f(\nu)$ is discussed below. Notably, the bending stress intensity factors asymptotically vary with $\sqrt{\lambda}$ instead of the typical $\sqrt{L}$.

There is some discrepancy in the literature concerning the precise values of the function $f(\nu)$. ? cites ? who both note that f is of order unity but do not give its exact form. ? appears to have first given the dependence of f on ν although ? found a mistake in this work. Meanwhile, ? gives a different value of f. It appears, however, that ? did not correctly account for the rift-wall boundary condition. Given this uncertainty and the additional detail involved in the ~~three dimensional~~ three-dimensional problem beyond the assumptions made by the above authors, I instead simply choose to calculate the value of $f(\nu)$ from the ~~three dimensional~~ three-dimensional calculations. From these calculations, I find a value $f(\nu = 0.3) = 0.7646$. Of the above references, this value is most similar to the value calculated from the equation given by ?, $f(\nu = 0.3) = 0.6063$.

Bending also creates a Mode-III stress intensity factor. Assuming that this bending can also be described within Euler beam theory, the Mode-III and Mode-I stress intensity factors are related by a factor,

$$\frac{K_{III}^b}{K_I^b} = \frac{h}{2\sqrt{2}(1+\nu)\lambda}. \tag{22}$$

Thus $K_{III}^b \sim h^2$, which is a larger exponent than for K_I^b. This solution was derived by assuming, consistent with Equations ??-??, that the ratio of stress intensity factors is proportional to the ratio of the stresses. This stress ratio is then calculated using the solution to the floating beam equation (?), $w = -2m_0/(\rho g \lambda^2)\exp(-x/\lambda)(\cos y/\lambda - \sin y/\lambda)$. The analytical solution of Eq. (??) is compared to the finite element solution in Fig. ??~~e~~ E (red dashed lines).

The analytical solution is not expected to perfectly match the finite element solution because the latter accounts for the full floatation condition (Eq. **??**), whereas the bending model (Eq. **??**) neglects higher order moments through Eq. (**??**). I further verify that the simplified model captures the behavior of the ~~three dimensional~~ three-dimensional simulations by calculating stress intensity factors over a range of ice shelf thickness between 25 m and 1600 m. I find that $K_I^b \sim h^{1.31}$ in the ~~three dimensional~~ three-dimensional calculations whereas $K_I^b \sim h^{1.375}$ analytically. Similarly, $K_{III}^b/K_I^b \sim h^{0.27}$ in the ~~three dimensional~~ three-dimensional calculations whereas $K_{III}^b/K_I^b \sim h^{0.375}$ analytically. As can be seen in Fig. **??**, the differences are more pronounced for K_{III}^b. I attribute the differences between analysis and calculation to the neglect of higher order moments and stress terms (i.e., the use of Euler beam theory).

4.1.2 The membrane components of ~~fracture~~the SIFs

~~In order to capture geometrical effects in a generic way, I introduce the following non-dimensionalization to~~ I carry out simplified two-dimensional finite element calculations in order to describe the membrane ~~modes of fracture. I define the geometrical factors χ and ψ, through the relationship~~

$$\chi = \sigma_m \sqrt{\pi L},$$

~~where σ_m is the depth-integrated boundary condition given in~~ components of the stress intensity factors. In two horizontal spatial dimensions x and y, the governing equations for the two-dimensional calculations are found by taking $\partial/\partial z = 0$ in Eqs. **??**-**??**. In two spatial dimensions, the boundary condition on floating ice fronts takes the stress value given by Eq. (**??**). ~~In this expression K_I^m and K_{II}^m are calculated as the depth-average of the finite element solution. Two comments are necessary about χ and ψ. First, the approximate depth-independence of the membrane components of fracture suggests that these quantities may be calculated in simplified,~~

I find good agreement between two-dimensional ~~elasticity simulations.Verification of the two-dimensional approximation is presented in Appendix A. Second, although the expressions in Equations **??** and **??** depend on the rift length L, the values~~ calculations and the depth-averaged values from three-dimensional calculations. Table **??** presents these results using the geometrical factors $\chi = K_I^m/(\sigma_m\sqrt{\pi L})$ and $\psi = K_{II}^m/(\sigma_m\sqrt{\pi L})$, where σ_m is the depth-integrated boundary condition given in Eq. (**??**). Note that $K_I \sim K_{II} \sim \sqrt{L}$ suggests that χ and ψ do not depend on L ~~. This is because K_I^m and K_{II}^m are expected to have a $\sqrt{L}$ dependence (**?**), therefore giving no net dependence on L.~~

~~Typical three-dimensional stress intensity factors as a function of depth z in the ice shelf. A. and B. show the Mode I stress intensity factor K_I, D. shows the Mode II stress intensity factor K_{II} and E. shows the Mode III stress intensity factor K_{III}. The associated sense of motion for each mode is shown in panels C, F, and G. B. has the mean removed and is compared to the analytical solution of Eq. (**??**). The geometrical parameters for this simulation are given in the text.~~

4.2 ~~Marginal rifts~~

Rifts originating in the ice shelf margins are examined in (?). The agreement is better for χ than for ψ, with differences on the order of several percent. This table also shows the effect of varying the maximum near-tip element length m. The values in this table are calculated for a central rift in an embayment with strong margins (i.e., as shown in Fig. ??, which plots the stress intensity factors $K_I(z=h)$ and $K_{II}(z=h)$ as a function ??D).

4.2 Central and Marginal Rifts

I now use the two-dimensional approach described in Section ?? to examine the effect of rift position for each of the three types on rift stability. I again consider all of the combinations of boundary conditions . Marginal ice shelf rifts become unstable in and rift locations shown in Fig. ?? while additionally varying the streamwise position of the opening mode as they pass into the region with weak margins or onto an ice tongue (at a position $\alpha = 0.5$). The similarity of the ice tongue and weak margin scenarios suggests that margin shear stress and not margin normal stress is the critical factor in determining the energy release rate and hence rift stabilityrift W.

Both the weak margin and ice tongue scenarios give rise to a compressive arch. The compressive arch is defined as the region where an ice shelf transitions from uniaxial to biaxial extension (?). The compressive arch can be visualized by plotting the second principle horizontal strain field, the first principle strain alway being positive Stress intensity factors for marginal rifts are plotted in Fig. ??. These stress intensity factors were calculated using the 2D parameterization described in Section ??. Consistent with the shearing stresses experienced in the ice shelf margins, the Mode I and Mode II stress intensity factors are of similar magnitude (Fig. ??). The specific simulation plotted in ??A and B, respectively). Fig. ?? is for the weak margins geometry (yellow curve ??C shows that marginal rifts always tend to propagate in the direction away from the ice front, i.e., in the positive y direction (coordinates shown in Fig. ??)with a rift located at $W/L_y = 0.57$. This is smallest distance from the ice front where rifts are stable. The compressive arch varies in position between $W/L_y = 0.50$ near the margins and $W/L_y = 0.62$ near the center.The stability condition is therefore found to approximately relate to the position of the compressive arch, with the exact stability threshold occurring before the rift actually crosses the arch. ??).

Although the Mode-I stress intensity factor changes from stable $K_I < K_c$ to unstable $K_I > K_c$ as a function of rift position α, the Mode-II stress intensity factor has a different interpretation. This shearing mode is unstable when $|K_{II}| > K_c$ and Marginal rifts are unstable over the greatest range of locations in the sign of K_{II} simply indicates the direction of shearing. With this interpretation in mind, the results in Fig. ?? suggest that marginal rifts –anywhere in the ice shelf– are unstable in the shearing mode (i.e., $K_{II} > K_c$ for all α) The most likely explanation for this apparent instability is simply that, although the rift is unstable in the prescribed orthogonal geometry, upon a small amount of propagation it will followed a curved path so as to minimize K_{II}. This point is discussed in more detail in the Discussion sectionice tongue and weak margin geometries (Fig. ??D). Specifically, they become unstable at a position $W/L_y \approx 0.66$. Stability in these geometries is not spatially monotonic, however, and rifts again become stable near the ice front at $W/L_y \approx 0.33$. Marginal rifts in ice shelves with strong margins, in contrast, have monotonically varying optimally oriented Mode I SIFs: they are stable near the grounding line and they become unstable at a distance $W/L_y \approx 0.33$ from the ice front.

~~Marginal rifts in ice shelves may be either stable or unstable depending on their position and on the marginal boundary conditions. This figure plots K_I/K_c in panel A and K_{II}/K_c in panel B. K_{III} is expected to not vary spatially and is therefore not plotted. All values are evaluated at the surface of the ice shelf $z = h$.~~

4.3 ~~Central Rifts~~

~~Rifts originating in the center of an ice shelf are examined~~ Stress intensity factors for central rifts are plotted in Fig. **??**~~, which also plots the stress intensity factors $K_I(z = h)$ and $K_{II}(z = h)$ as a function of rift position for each of the three types of boundary conditions~~. In contrast to the marginal rifts, central rifts have $|K_{II}| \ll |K_I|$ (Fig. **??**A and B). Unlike marginal rifts, propagation angles are smaller, indicating nearly straight-ahead propagation (Fig. **??**C). Furthermore, central rifts in all positions ~~and with all boundary conditions~~ are found to have negative ~~K_I and far smaller K_{II}, therefore suggesting the stability of this configuration. Although values of K_{II} approach K_c, given the uncertainty in values of the fracture toughness K_c (?) and given the order of magnitude greater~~ optimally oriented stress intensity factors ~~for marginal rifts, I therefore do not interpret this as a common or significant source of instability.This point is also discussed at greater length in the next Section~~indicative of stability (Fig. **??**D).

5 Discussion

I have presented a three-dimensional LEFM analysis of ice shelf rift propagation. ~~The~~ While this model has many potential applications, I have focused on the relationship between rift position and rift stability. In that regard, the main result of this analysis is that rifts originating in the margins of ice shelves become unstable if the ice shelf margin looses shear strength. This transition between a strong margin and a weak margin can be seen, for example, by comparing the red and yellow curves in Fig. **??**D. Although this result is justified by the calculations presented in this paper, it is worth emphasizing several implicit and subtle assumptions.

I have assumed that margins have either zero displacement or zero shear stress. In reality, margins likely experienced reduced but nonzero shear stress. I have also considered only two rift locations (marginal or central), only one ice shelf geometry (square), and only one rift geometry (a single rift, perpendicular to flow, and without curvature). I treat the entire ice column as having identical material properties and therefore do not describe the firn layer and its relation to partial contact of rift walls. Additional observed rift-wall processes such as brine infiltration, surface accumulation, and variable uplift could also be investigated (**???**). Each of these assumptions deserves further examination. ~~In particular, I anticipate that future work will examine the path along which fractures will tend to propagate (???). Nevertheless,~~ Despite these limitations, ice shelves and ice shelf rifts oftentimes approximately conform to ~~these assumptions , and so I~~ the assumptions described in this study. I do therefore expect that the results presented here ~~are a useful starting point in understanding additional aspects of~~ provide a useful basis for understanding rift propagation.

5.1 ~~A simplified rift propagation criterion based on flexural stabilization~~The compressive arch

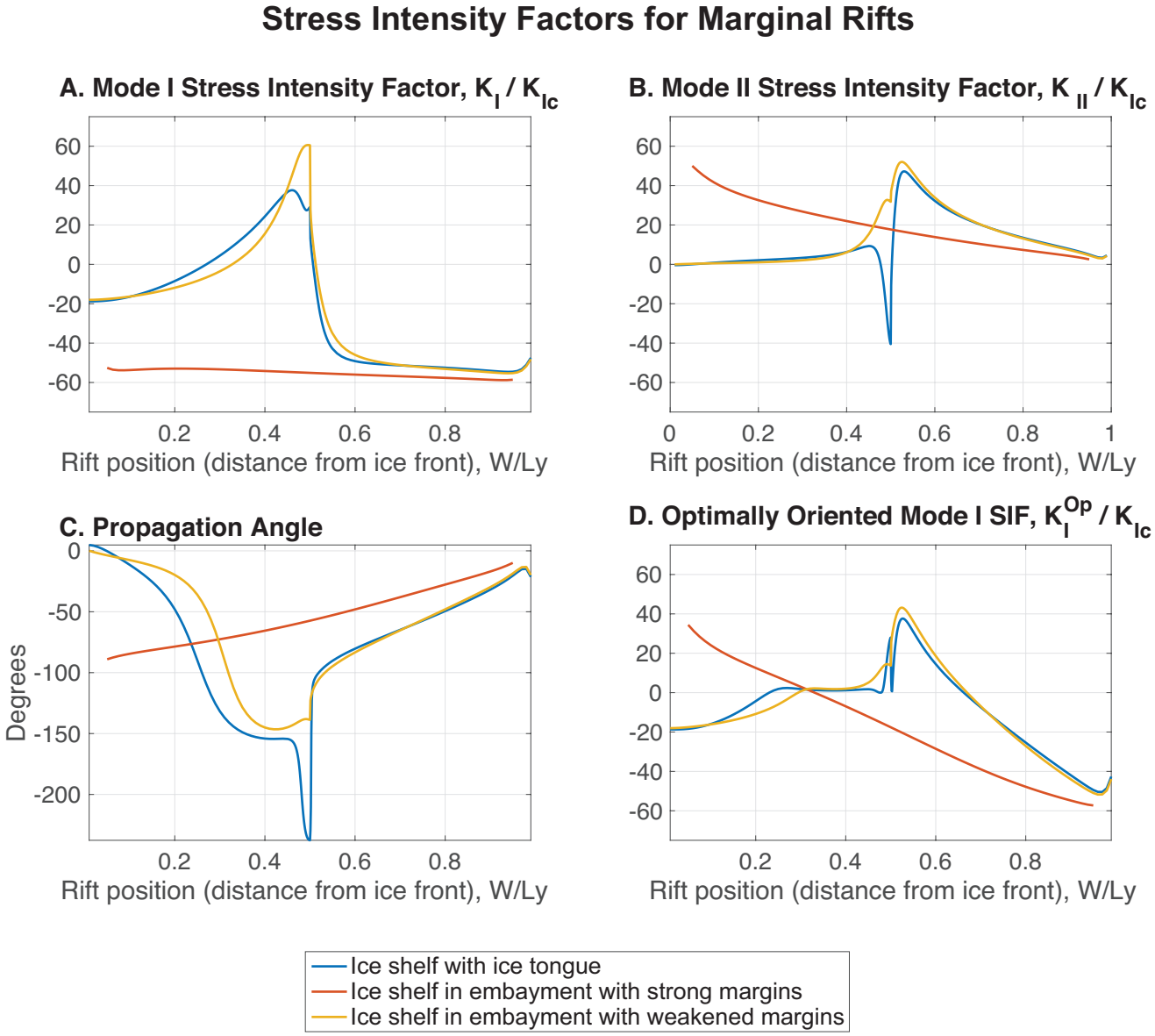

Figure 4. ~~The ice shelf compressive arch (dashed line) distinguishes regions~~ Stress intensity factors for marginal rifts may reflect either stability or instability depending on the position of ~~uniaxial and biaxial extension. This occurs as~~ the ~~boundary where the second principal strain experiences a zero crossing. The~~ rift~~location shown in this figure is in~~ . Three pieces of information, the ~~closest stable distance to the ice front~~A. Mode I SIF, ~~which for a square ice shelf is calculated to be $W/L_y = 0.57$~~B. ~~If this rift were shifted slightly closer~~ Mode II SIF, and C. Propagation angle, are combined using Eq. (**??**) to calculate D. the ~~ice front it would grow in an unstable manner~~optimally-oriented SIF.

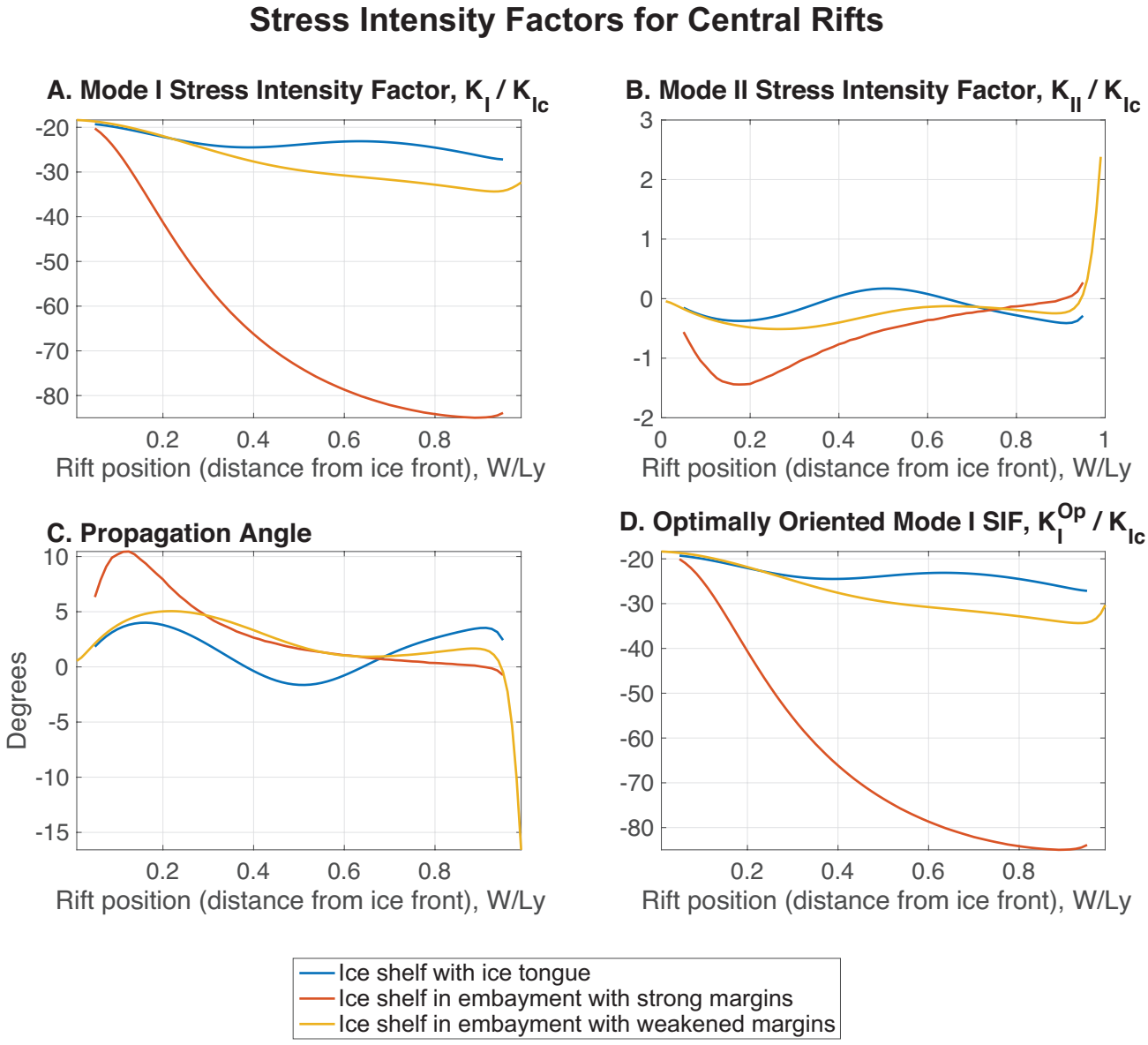

Figure 5. ~~Central~~ Stress intensity factors for central rifts ~~in ice shelves are always found to be stable, regardless~~ reflect stability for all rift positions. Three pieces of ~~their position or~~ information, the ~~marginal boundary conditions. This figure plots K_I/K_c in panel~~ A~~and K_{II}/K_c in panel~~. Mode I SIF, B. ~~K_{III} is expected to not vary spatially~~ Mode II SIF, and ~~is therefore not plotted~~C. ~~All values~~ Propagation angle, are ~~evaluated at~~ combined using Eq. (**??**) to calculate D. the ~~surface of the ice shelf $z = h$~~optimally-oriented SIF.

~~The results in Section ?? suggested the approximations $G_c/G \approx 0$ and $K_{III}, K_{II} \ll K_I$. I combine these approximations with the general fracture criterion (Eq. ??) and the components of K_I (Eq. ??), and evaluate the result at $z = h$, which is expected to be the most difficult part of~~

All boundary conditions considered here give rise to a compressive arch, defined as the region where an ice shelf transitions from uniaxial to biaxial extension (?). The compressive arch can be visualized by plotting the second principle horizontal strain field, the first principle strain alway being positive (Fig. ??). ? proposed that "once a retreating ice front breaks through the critical 'compressive arch' then retreat is irreversible." The results presented here broadly confirm the hypothesis of ?, although as shown in Section ??, the relation to the compressive arch only holds in an approximate sense. Specifically, for the strong margin boundary condition the ~~rift to break. The resulting fracture criterion is,~~

$$\chi \sigma_m \sqrt{\pi L} \geq \sigma_b f(\nu) \sqrt{\lambda}.$$

~~This condition has the interpretation that flexurally-induced partial contact of rift walls acts in a manner similar to the fracture toughness K_c insofar as it is a resistance to rift growth that does not depend on rift length L.I refer to this phenomenon as flexural stabilization. This condition may be further simplified by using Equations ?? and ??,~~

$$L \geq \begin{cases} \chi^{-2} F(\nu, \rho/\rho_w) \lambda \equiv L_c & \chi > 0, \\ \infty & \chi < 0, \end{cases}$$

~~where F is a function that depends only on Poisson's ratio ν and ρ/ρ_w.For $\nu = 0.3$ and $\rho/\rho_w = 0.89$, $F = 0.0716$. The expression of Eq. (??) defines the critical rift length for stability L_c. It has the interpretation that rifts are expected to grow unstably when they exceed a length L_c proportional to the flexural length λ. For the case shown in~~ onset of instability occurs somewhat upstream from the maximum extent of the compressive arch (Fig. ??A.). For the weak margins and ice tongue boundary conditions the agreement is closer, however, there is also a region of stability that occurs closer to the ice front (Fig. ??, ~~$\chi = 0.55$, giving $L_c = 217$ m.However, given such a small L_c, in many cases of practical glaciological importance $\chi > 0$ may well approximate the criterion for rift propagation .~~ ??B. and C.).

Perhaps more importantly, the results presented here suggest a slightly different order of causality than that proposed by ?. Rather than being an independent boundary that rifts may or may not propagate through, rift propagation in the model presented here is expected to occur precisely because of the stress state that creates the compressive arch. Ice shelf retreat is expect to be irreversible only insofar as marginal weakening is itself irreversible.

5.2 Melange as a rift proppant

? observed a lack of rift-tip seismicity at central rift in the Ross Ice Shelf. This observation is consistent with the negative ~~K_I~~ K_I^{Op} I have calculated for centrally-located rifts. In the absence of other forces such rifts will tend to close. It seems likely that these rifts therefore owe their continued existence to rift-filling melange that acts as a type of proppant by holding the rift open. Melange therefore has a dual nature. ? and ? showed that melange maintains shear stresses and therefore resists viscous

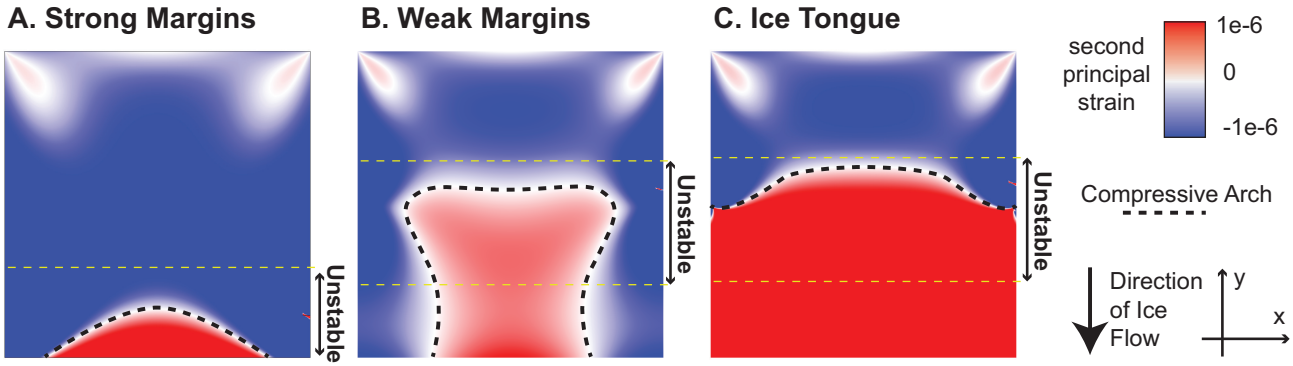

Figure 6. The ice shelf compressive arch (thick black dashed line) is plotted for three boundary conditions: A. Strong Margins, B. Weak Margins, and C. Ice Tongue (see Fig. **??**). The figure also shows the boundaries of regions of rift instability (thin yellow dashed lines). These figures were calculated in two horizontal spatial dimensions as described in Section **??**.

flow. In this sense, melange is stabilizing. Yet in the sense that melange may sometimes enable the existence of rifts that would otherwise close, melange is destabilizing.

5.3 Wave-induced fracture

? used passive seismic data to calculate the elastic ice shelf stresses due to ocean swell acting on the Ross ice shelf. This study concluded that some un-modeled process must have been operating in order to explain the lack of any observed ice shelf rift propagation during the observation period. Specifically, **?** calculated a maximum wave-induced Mode-I stress intensity factor $K_I \approx 2$ MPa m$^{1/2}$ for a site near the Nascent Iceberg Rift. Using the results presented here for a central rift, we calculate that for a near-front central rift with $W/L_y = 0.05$, the Mode-I stress intensity without wave stress would be ~~$K_I \approx -5$~~ $K_I^{Op} \approx -5$ MPa m$^{1/2}$. The resulting total Mode-I stress intensity factor of ~~$K_I \approx -3$~~ $K_I^{Op} \approx -3$ MPa m$^{1/2}$ being negative is consistent with the observation that ocean swell did not trigger rift propagation during the observation period described by **?**.

5.4 ~~The compressive arch~~

~~**?** proposed that "once a retreating ice front breaks through the critical 'compressive arch' then retreat is irreversible." The results presented here broadly confirm this hypothesis, although as shown in Section **??**, the relation to the compressive arch only holds in an approximate sense. Perhaps more importantly, the results presented here suggest a slightly different order of causality than that proposed by **?**. Specifically, my results imply that rift propagation occurs precisely when the rift breaks through the compressive arch. Rifts on the landward side of the compressive arch, in contrast, are not expected to experience propagation. Ice front retreat following is therefore expected to be irreversible as hypothesized by **?**. Future marginal~~

~~strengthening, however, would cause a seaward migration of the compressive arch, therefore permitting a certain notion of reversibility. Future work will investigate the propagation paths taken by ice shelf rifts with respect to the compressive arch.~~

6 Conclusion

I have modeled an ice shelf as a three-dimensional buoyantly floating elastic plate. ~~The resulting calculationsshow that through-cutting~~ I then show how these three-dimensional results may be captured in simplified two-dimensional calculations. Using the two-dimensional theory, I show that ice shelf rifts become unstable in the presence of marginal weakening or upon exiting an embayment. These results are a step towards prognostic ice shelf modeling with a physics-based relationship between ice dynamics and an ice front extent set by rift propagation.

Code and data availability. The analysis code used in the text is available on the author's GitHub repository.

7 ~~Numerical implementation~~

6.1 ~~Discretization~~

~~The ice shelf domain is discretized using a free tetrahedral mesh in three spatial dimensions or a free triangular mesh in two spatial dimensions. In the three dimensional simulations, the maximum element size along the rift is set to be $h/16$. The element size then increases away from the rift to a maximum value of 3.5 km. The rift is geometrically formed as a rectangular prism with width $W_{\text{rift}} = 10$ m and length L. I have verified that the results presented here have virtually no dependence on the choice of W_{rift}, provided that the value is chosen to be sufficiently small. In the two dimensional simulations (described below), the maximum element size along the rift is $W_{\text{rift}}/10$.~~

6.1 ~~Stress intensity factor calculations~~

~~Stress intensity factors are directly evaluated using the asymptotic solution of Equations **??**- **??**. This evaluation method is sometimes called the displacement correlation method (**?**) and has previously been used in glacier studies by **?**. In three dimensions, displacement differences across the rift are calculated at various heights through the ice shelf thickness, with the resulting calculations plotted in Fig. **??**.~~

~~The uniformity of K_I^m and K_{II}^m with depth permits simplified two-dimensional elasticity calculations of these quantities. In two dimensions, displacement differences across the rift are calculated at a single set of points. A comparison of the geometrical parameters χ and ψ calculated in two and three spatial dimensions is presented in Table **??**. The agreement is better for χ than for ψ, with differences on the order of several percent.~~

~~Comparison between 2D and 3D calculations$h$ 2D 3D Δ (2D-3D)/3D χ 100 m -0.2937 -0.3127 12.5 m -6.1% 200 m -0.2937 -0.3012 5 km -2.5%200 m -0.2937 -0.3069 12.5 m -4.3%ψ 100 m-0.04408-0.0385 12.5 m +14.5%200 m -0.04408 -0.0382 5 km +15.4%200 m -0.04408 -0.0379 12.5 m +16.3%~~

Competing interests. The author declares that no competing interests are present.

Acknowledgements. This project began with a discussion with Colin Meyer at the Cambridge symposium of the International Glaciological Society in 2015. Jim Rice and Eric Dunham read earlier versus of this manuscript and gave the author helpful comments. Several discussions with Brent Minchew, Jan De Rydt, and Hilmar Gudmundsson also helped along the way. On a visit to C.U. Boulder organized by Jed Brown, David Marshall was critical of some early results; this feedback was helpful. The author was funded by the Department of Earth and Planetary Sciences at Harvard University.